Improving the performance of pseudo-ductile hybrid composites by film-interleaving
Marino S. G., Czél G.

Composites: Part A 142 (2021) 106233

Contents lists available at ScienceDirect

Composites Part A

journal homepage: www.elsevier.com/locate/compositesa

Improving the performance of pseudo-ductile hybrid composites by film-interleaving

Salvatore Giacomo Marino, Gergely Czél *

Department of Polymer Engineering, Faculty of Mechanical Engineering, Budapest University of Technology and Economics, Műegyetem rkp. 3, H-1111 Budapest, Hungary

ARTICLE INFO

Keywords:
A. Hybrid
B. Fragmentation
B. Fracture toughness
B. Delamination

ABSTRACT

Improvement of the interfacial fracture toughness of the layer interfaces is one way to increase the performance of interlayer hybrid laminates containing standard thickness carbon/epoxy plies and make them fail in a stable, progressive way. The layer interfaces were interleaved with thermoset 913 type epoxy or thermoplastic acrylonitrile–butadienestyrene (ABS) films to introduce beneficial energy absorption mechanisms and promote the fragmentation of the relatively thick carbon layer under tensile loads. Carbon layer fragmentation and dispersed delamination around the carbon layer fractures characterised the damage modes of the epoxy film interleaved hybrid laminates, which showed pseudo-ductility in some cases. In the ABS film interleaved laminates, a unique phase-separated ABS/epoxy inter-locking structure was discovered at the boundary of the two resin systems, which resulted in a strong adhesion between the fibre-reinforced and the thermoplastic layers. As a result, the delamination cracks were contained within the ABS interleaf films.

1. Introduction

Fibre-reinforced polymer composites (FRPCs) are particularly attractive for high performance structural applications (e.g. automotive, aerospace, etc.) due to their high strength-to-weight ratio. However, FRPCs fail in a brittle manner, without sufficient warning before failure, in contrast to most of the traditional engineering materials, such as metals, usually characterised by ductile behaviour. In order to make composite structures safe enough, they are often oversized. In this way, their excellent strength/weight ratio is not fully exploited. Recent studies [1–4] in pseudo-ductile hybrid composite materials have demonstrated the possibility to reproduce the metal-like ductile failure in FRPCs, and design structures with a wide safety margin before the typical catastrophic failure. Pseudo-ductility in FPRCs was achieved in well-designed material configurations of thin-ply continuous unidirectional (UD) fibre-reinforced interlayer hybrid composites [1,5], and in tailored architectures incorporating discontinuous layers [6–9], angle-ply laminates [10–12] and short fibre hybrid composites [13–15]. Contrarily to the ductility of metals, pseudo-ductility in hybrid composites is characterised by a gradual and diffused failure of one of the constituents, which has a lower strain to failure than the other one. Czél and Wisnom [1] demonstrated that, in continuous carbon/glass fibre-epoxy interlayer hybrid composites, pseudo-ductility is generated by the fragmentation (i.e. multiple fractures) of the thin carbon reinforced layer. The general conditions to achieve fragmentation are i) high mode II interlaminar fracture toughness (G_{IIC}) of the layer interfaces and ii) low strain energy release rate at the first fracture of the carbon/epoxy layer [2]. Tough interfaces can absorb the energy released at the fracture and unloading of the thin carbon layer, preventing sudden delamination and allowing the carbon layer to fragment progressively. Thin carbon layers allow fragmentation, but the extra stiffness added to the hybrid laminates is minor. Higher stiffness increment is achievable with thicker carbon layer and higher carbon/glass volume ratio, but these configurations release higher energy at the first fracture which promote catastrophic delamination if the interfaces are not tough enough. Interfacial toughening may allow for higher added stiffness and pseudo-ductility by using standard thickness carbon plies and increased carbon/glass ratios. Furthermore, standard thickness carbon plies are significantly cheaper than thin ones, which can make pseudo-ductile hybrid composites more attractive for practical applications.

The strategies to increase the G_{IIC} in composites involve the introduction of beneficial energy absorption mechanisms for delaying or suppressing delamination, i.e. crack arresting or crack path deviating mechanisms. For example, approaches like nanofibrous layer

* Corresponding author.
E-mail addresses: marinos@pt.bme.hu (S.G. Marino), czel@pt.bme.hu (G. Czél).

https://doi.org/10.1016/j.compositesa.2020.106233
Received 25 September 2020; Received in revised form 18 November 2020; Accepted 2 December 2020
Available online 15 December 2020

interleaving [16–21] or the use of carbon nanotube (CNT)-modified epoxy matrices [22–25] were effective in toughening fibre-reinforced laminates. However, thick interleaf layers [18] or high CNT concentration [23] may lead to the saturation of the toughening effect or could even become detrimental to the overall laminate performance. Interleaving the stiff fibre reinforced composite layers with flexible thermoplastic layers may increase the delamination tolerance of the resulting material if the bonding between the constituent materials is sufficient. The fracture energy absorbed by the interleaved layers retards, or suppresses, the interlaminar crack propagation [26–30]. Furthermore, flexible film interleaves are particularly suitable for high-performance applications, where structural components are usually fabricated from prepregs [31,32].

Thermoplastic film interleaves aim to create a phase-separated blend with the base epoxy matrix in the composites. The phase-separation characterised morphology promotes good bonding between the interleaf and the composite layers and generates energy dissipation mechanisms which contribute to increasing the material's fracture resistance [33,34]. Thin film interleaves do not reduce the mechanical properties of the composite material (i.e. elastic modulus) significantly [35,36].

Extra resin film layers made of the same resin used to embed the reinforcing fibres have improved both G_{IC} and G_{IIC} in numerous studies. Singh et al. [37] showed an increase of up to 70% for mode I, and 200% for mode II fracture toughness by interleaving the carbon/epoxy prepregs (Fibredux 927), with 50 μm and 200 μm thick layers of the same matrix resin. Similarly, Hojo et al., [38] registered superior performances in both static and fatigue tests due to the improved G_{IIC} in their matrix film interleaved carbon FRPCs (Toho UT500/111). The fracture morphology of epoxy interleaved laminates under mode II loading revealed larger damage zones characterised by micro-crack bifurcation mechanisms than those of the reference composite materials. Ionomer films can also increase the G_{IIC} through interleaving flexible films in composites [39]. The toughening effect is based on the chemical compatibility between the end-groups of the ionomer film and the epoxy matrix, enhanced further by heating and melting the ionomer films in a post-curing cycle [40].

Evidences for the toughening effect of acrylonitrile butadiene styrene (ABS) in epoxy blends or FRPCs were presented in the technical literature [41–45], although these studies used ABS not in film form (e.g. particles), and they have applied particle dispersion and dissolution based sample preparation processes not lamination, the most conventional composite manufacturing process. On the other hand, Robinson et al. [46,47] applied thick interleaves of polystyrene (PS), which has a similar chemical character to ABS, for developing controllable stiffness FRPC laminates. They confirmed sufficient bonding between the carbon/epoxy and the thermoplastic layers during repeated shape-memory experiments therefore we expect good adhesion between ABS and fibre reinforced epoxy layers. Although the literature on the interleaving effect in traditional FRPCs is rich, there are no study, to the best of our knowledge, that investigates the combined effect of interleaving and fibre hybridisation to achieve pseudo-ductility. This paper evaluates the possibilities of promoting pseudo-ductility in UD interlayer hybrid composites made with standard thickness carbon/epoxy plies by film interleaving with epoxy resin or ABS films. We selected ABS because it has lower T_g than other common interleaf materials (e.g. PES, PSU, PEI) and the curing temperature recommended for the epoxy system used here (i.e. 125 °C) therefore processing conditions enabling good integrity of the layers (i.e. softening of the interleaf films) are provided. We expected chemical compatibility and sufficient adhesion between the constituents based on the technical literature. We also decided to use films of the same epoxy as the matrix of the composite layers in the hybrid laminates as interleaf layers for maximum compatibility. Standard, well established constituent materials are key to timely penetration of new technologies to real applications (e.g. wing panels, wind turbine blades), therefore standard thickness carbon/epoxy was used in our study, as it is also significantly cheaper and simpler to obtain than special thin plies.

2. Concept, configuration design and materials

This section provides details of the motivation, challenge, approaches, available material systems and design considerations for our study.

2.1. Concept

Fibre hybrid composite materials balance the mechanical properties of two fibre constituents (e.g. carbon and glass) both embedded in a common epoxy matrix. Hybridisation may be useful for optimising the performance of the resulting material, in terms of damage mechanisms, exploiting the advantages of the single fibre constituents [48]. The laminates studied here were made by interlayer hybridisation, i.e. "sandwiching" UD continuous carbon/epoxy between glass/epoxy plies, as shown in Fig. 1.

The different elastic moduli and strain to failure of the constituents generate a multistage damage process in hybrid laminates, as schematically shown in Fig. 2. Then, the tensile stress-strain curve is characterised by an initial linear stage followed by a transition stage, in which the fracturing process of the low strain material (LSM) may results in sudden delamination or progressive fragmentation, according to the energy released by its damage. Pseudo-ductility was observed in continuous UD carbon fibre/glass fibre-epoxy interlayer hybrid composites [1], by exploiting the different strains to failure and elastic moduli of the thin carbon/epoxy and standard glass/epoxy plies. Pseudo-ductility is characterised by multiple fractures (i.e. fragmentation) of the LSM and a stable pull-out from the HSM layers under tensile load, and prevent the samples from sudden spreading of delamination and the corresponding major stress-drop. As soon as the fragmentation process saturates, the high-strain material (HSM) takes the full tensile load up to final material failure.

In [1,5], Czél demonstrated that pseudo-ductility based on the fragmentation of a thin carbon layer is governed by the following inequality:

$$G_{IIC} > G_{II} = \frac{\varepsilon_{2b}^2 E_c t_c (2E_g t_g + E_c t_c)}{8E_g t_g} \tag{2.1}$$

where ε_{2b} is the tensile strain to failure of the carbon/epoxy layer (estimated by the fibre failure strain for design purpose), E_g and E_c are the tensile moduli of the glass/epoxy and the carbon/epoxy layers, respectively; t_g and t_c are the thicknesses of the glass/epoxy and the carbon/epoxy layers, respectively (see Fig. 1).

Inequality 2.1 means that the mode II energy release rate (G_{II}) at the first fracture of the carbon layer must be lower than the mode II interlaminar fracture toughness (G_{IIC}) to prevent delamination of the layers of the hybrid laminate. The thicknesses of the LSM and HSM control the G_{II} and affect the damage mode of the hybrid laminate.

2.2. Applied composite materials

The FRPC plies used to manufacture the hybrid laminates were IM7 carbon/913 epoxy and S-glass/913 epoxy prepregs, provided by Hexcel in 300 mm wide rolls. The fibres in both the carbon and the S-glass prepregs were impregnated by the same epoxy matrix, i.e. HexPly 913 (Hexcel), so there were no compatibility issues when processing the different plies together. The mechanical properties of the dry fibres are reported in Table 1; the properties of the cured plies are listed in Table 2.

2.3. Applied interleaf films

The studied hybrid composites were interleaved with 30 μm and 60 μm nominal thickness 913 epoxy (Hexcel) and Starex LX0981

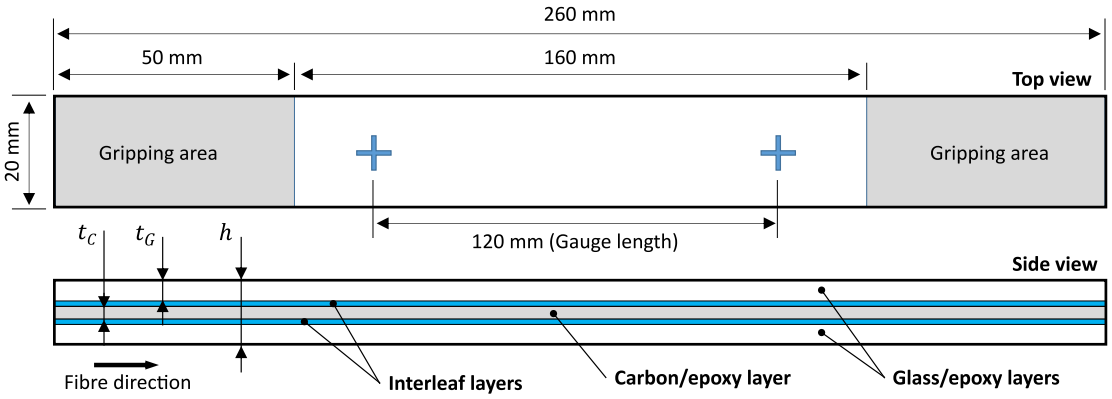

Fig. 1. Geometry of the interlayer hybrid specimen. The grey coloured areas in the top view are the gripping areas covered by sandpaper. The side view shows the stacking sequence of the interleaved hybrid composite; the baseline material has the same architecture but without the interleaf layer. (For interpretation of the references to colour in this figure legend, the reader is referred to the web version of this article.)

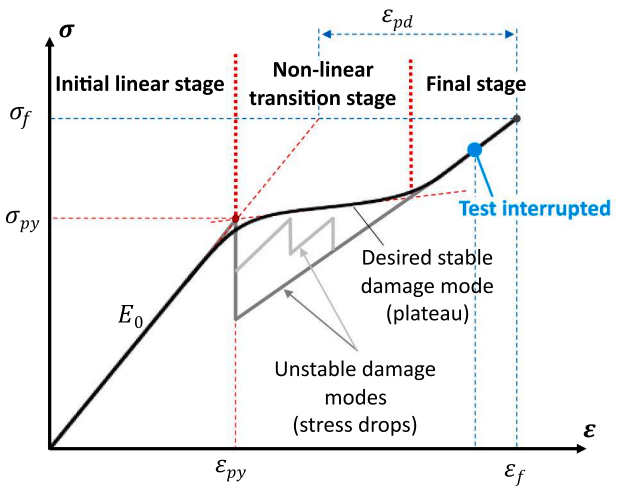

Fig. 2. Possible tensile stress-strain curves of hybrid laminates, and definition of the test stages. In the non-linear transition stage, the damage modes of a hybrid composite that can occur with the fracture of the low strain constituent are represented. (For interpretation of the references to colour in this figure legend, the reader is referred to the web version of this article.)

acrylonitrile–butadienestyrene (ABS) films (Lotte Chemical, South Korea). The epoxy film was selected to be the same as the matrix system of the applied prepregs, and it was provided directly in a film format on a 300 mm wide roll. The ABS film was produced from pellets by extrusion. The extruder machine was a 25 mm diameter single screw Labtech LCR300 type (Labtech Engineering Co., Thailand) equipped with a 200 mm wide flat film die. The length/diameter ratio of the screw was l/d = 30. The zones of the barrel were in the temperature range of 210 to 225 °C, and the die was tempered at 230 °C. The pellets were dried at 80 °C for 4 h before extrusion according to the manufacturer's guidance. Table 3 reports the properties of interleaf films.

2.4. Design of test laminates

Jalalvand et al developed the concept of damage mode maps in [2,49–51], which is a tool that can be used for designing pseudo-ductile interlayer hybrid composite materials (see Fig. 1). The maps can be generated for a given material pair by using the mechanical properties of the constituents applied in the hybrid composite (i.e. elastic properties, strain to failure of the constituents and G_{IIC}). The damage mode maps are drawn on the basis of a parametric study of the damage modes the hybrid laminates may encounter in function of the thicknesses of the hybrid constituent layers, i.e. LSM and HSM. The possible damage modes predicted are *premature failure* (failure of the whole laminate together with the first fracture of the LSM); *catastrophic delamination* (sudden and full delamination after the first fracture of the LSM), *fragmentation + dispersed delamination* (multiple fracture of the carbon layer with stable delamination around the carbon layer fractures) and *fragmentation* (with no delamination). Fig. 3 (b) schematically shows the possible damage modes of the hybrid laminate and the regions of the map in which they are predicted to occur. We studied the damage modes of the carbon/glass–epoxy interlayer hybrid configurations through calculating the positions of the available configurations on the damage mode map based on their relative and absolute LSM thicknesses. To draw the boundary lines of the map, we needed the G_{IIC} of the hybrid material, which was determined experimentally through a separate series of tensile tests on specimens similar to the ones proposed by Wisnom [52] and Cui [53], with central-cut carbon/epoxy layer between continuous glass/epoxy layers. This architecture generates shear loads (inducing pure mode II crack propagation) at the discontinuous/continuous layer interfaces and allows for simple determination of the G_{IIC}. We tested three different layup configurations (six samples for each series), varying the relative thickness of the carbon/epoxy layer. The measured G_{IIC} is reported in Fig. 3(a), and the resulting average value (1.809 kJ/m^2) is used here for drawing the damage mode map. The configurations indicated on the damage mode map (see Fig. 3(b)) show

Table 1
Properties of the applied reinforcing fibres based on manufacturer's data.

Type	Manufacturer	Tensile elastic modulus [GPa]	Tensile strain to failure [%]	Tensile strength [MPa]	Density [kg/m^3]	Coefficient of thermal expansion *10^{-6} [1/K]
Y-110 S-2 Glass	AGY	89	5.7	4890	2470	2.9
HexTow® IM7 Carbon	Hexcel	276	1.9	5516	1780	−0.64

Table 2
Cured ply properties of the applied UD prepregs based on manufacturer's data.

Prepregs	Nominal fibre areal density [g/m^2]	Fibre volume fraction [-]	Cured ply thickness [μm]	Tensile strain to failure [%]	Tensile modulus [GPa]
S Glass/913	190	0.49	153.8	3.7[(a)]	45.6
IM7 Carbon/913	100	0.58	95.8	1.68[(b)]	163.2

[(a)] Measured in previous experiments on composites made of similar glass fibres with the same resin system [5].
[(b)] From HexPly® 913 product datasheet.

Table 3
Properties of the applied film interleaves based on manufacturer's data.

Material	Density [g/cm^3]	Nominal areal density [g/m^2]	Nominal thickness [μm]	Young's Modulus [MPa]	Glass transition temp. [°C]
Hexcel© 913 epoxy	1.23	34	30	3400	157
Starex® LX0981 ABS	1.05	31.5/63	30/60	2260	103[(a)]

[(a)] From DSC tests.

the hybrid configurations made by using a single continuous carbon ply as the LSM. This way, the absolute thickness of the LSM (i.e. t_c, see Fig. 1) was minimised. The three laminates analysed were designed varying only the relative thickness of the carbon layer by changing the number of the glass/epoxy plies. The configuration [G/C/G], which stands for glass (G)/carbon (C)/glass (G) plies in the layup sequence, is predicted to fail prematurely due to glass/epoxy layer fracture together with the first fracture of the carbon/epoxy layer (see Fig. 3(b)). Adding more glass/epoxy plies, the damage mode of the [G_2/C/G_2] hybrid material changes to *catastrophic delamination*, without the immediate glass layer failure at the first carbon layer fracture. The configuration [G_3/C/G_3] is also expected to delaminate catastrophically after the first fracture of the carbon layer, but it is less critical for glass/epoxy layer fracture. This last configuration is relatively close to the desired region of the damage mode map in which fragmentation of the carbon layer and dispersed delamination can occur. The parametric analysis reported in Fig. 3(c) shows that varying the G_{IIC} of the materials, shifts the lines which separate stable and unstable damage modes. Increasing the G_{IIC}, we predict that the configuration [G_3/C/G_3] will damage stably, i.e. enter the fragmentation zone of the map. On the contrary, the other configurations considered, i.e. [G_2/C/G_2] and [G/C/G], change their damage mode to *premature* failure. The aim of our study is to increase the G_{IIC} of the hybrid material, satisfy equation (2.1) and achieve fragmentation by

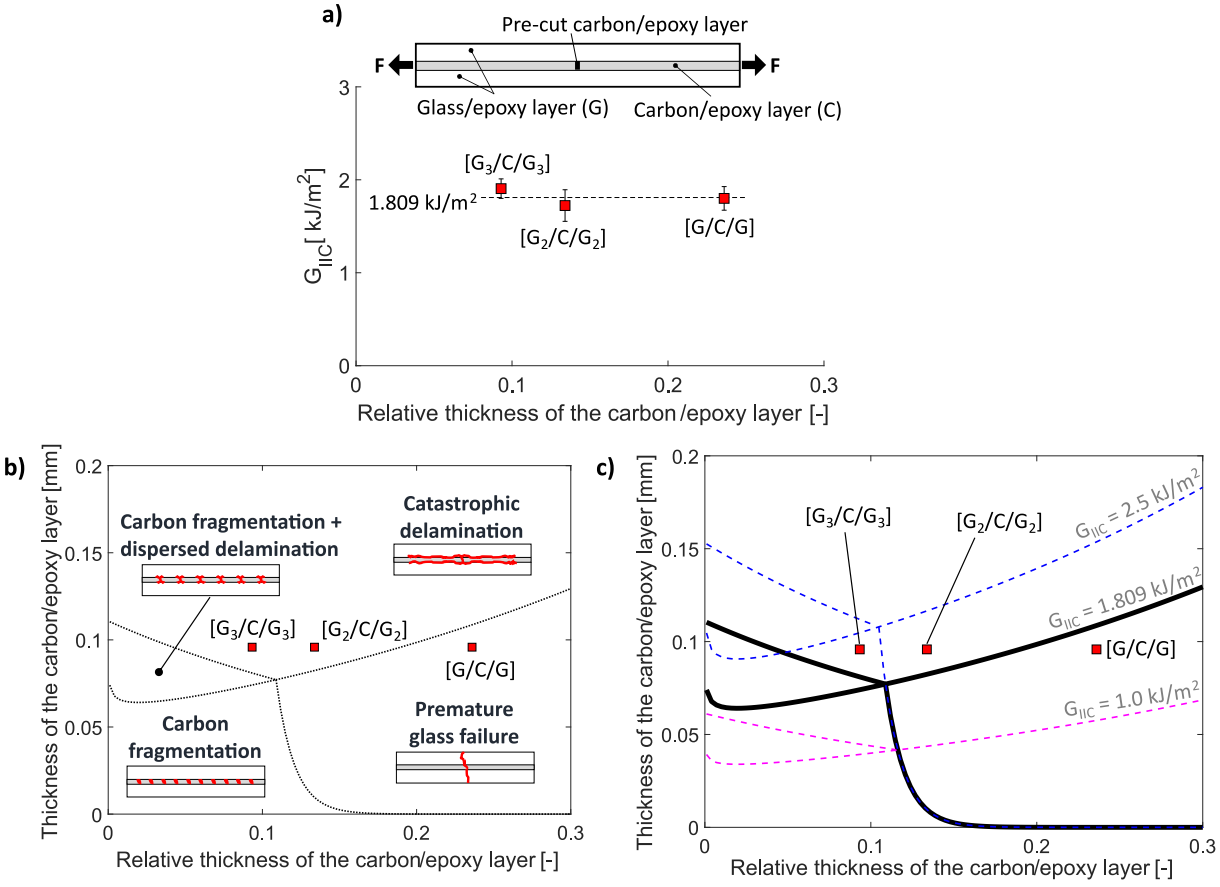

Fig. 3. (a) Measured G_{IIC} of the UD hybrid central-cut IM7 carbon/epoxy – continuous S glass/epoxy composites plotted against the relative carbon layer thickness (calculated with respect to the full thickness of the laminate). (b) Damage mode map related to the continuous IM7 carbon/S glass–epoxy material combination. (c) Parametric analysis of the damage modes in function of the G_{IIC} of the hybrid material. (For interpretation of the references to colour in this figure legend, the reader is referred to the web version of this article.)

toughening the interfaces of the hybrid laminate through interleaving to suppress, or delay, delamination. The configuration [G_3/C/G_3] is adopted here as the baseline and the interfaces between the carbon/epoxy and glass/epoxy layers are toughened by interleaving epoxy and ABS films, (see Table 4 for the list of tested configurations).

3. Test methods

3.1. Tensile tests

Uniaxial, quasi-static tensile tests were conducted on a computer-controlled Zwick Z250 type 250 kN rated universal electro-mechanic test machine fitted with a regularly calibrated 250 kN load cell and 100 kN rated Instron 2716-003 type manual wedge action grips. The crosshead displacement speed was set to 5 mm/min. Specimen geometry is highlighted in Fig. 1. Since the high strain S-glass/epoxy layers of the hybrid laminates were placed on the outside, it was possible to test the specimens without end-tabs. As the focus of the study was the analysis of the damage initiation in the carbon/epoxy layer and the following delamination related phenomena, the final failure strain of the laminates, still affected by stress concentration in the S-glass/epoxy layers at the grips, was not crucial. All the tests were interrupted at around 3% of strain to prevent the final failure of the samples and preserve their integrity (see Fig. 2) for further fracture mechanism analysis. The ends of the specimens were covered with 50 mm long P80 grit size sandpaper pieces with the rough side turned to the specimen surface to protect it from damage from the sharp nails of the grip faces, while maintaining sufficient friction to prevent the specimens from sliding out during loading (see Fig. 1). Six specimens were tested for each material configuration.

3.2. Optical strain measurement

The strain was measured with a Mercury RT type optical extensometer system with a 5 MPixel Mercury Monet camera (Sobriety, Czech Republic). The gauge length of the specimens (between the markers tracked by the extensometer) was set to 120 mm (see Fig. 1).

3.3. Microscope analysis

The scanning electron microscope (SEM) analysis of delaminated interfaces was performed with a JEOL JSM 6380 LA SEM (JEOL Ltd., Japan). The samples were sputter-coated with gold in a vacuum chamber for 30 s to avoid static charging during imaging.

Polished cross-sections of the damaged/failed samples were analysed with an Olympus BX51M type optical microscope (Olympus, Germany). For this purpose, the pristine and tested samples were cut with a diamond wheel and cleaned with compressed air to remove residual particles from the cut. The samples were embedded in epoxy resin that crosslinked in 24 h at ambient temperature. The resin blocks were polished in a Buehler Beta type machine with sandpaper and liquid suspensions of 9, 3 and 0.05 μm abrasive particle sizes. We analysed both cross-sections and longitudinal-sections of the samples. The optical microscope images of the baseline and epoxy film interleaved samples were taken by using the *bright field mode*, in which the light is perpendicular to the sample surface. The samples of the ABS interleaved configurations were analysed in *dark field mode*, where the light is oblique to the observed surface. In this case, the colours are more distinct in the resulting images.

ImageJ software was utilised to calculate the volume fraction of carbon fibres ($V_{f,c}$) in the cross-sectional images taken with the optical microscope. The carbon fibre contours were highlighted by sharpening the grayscale images and applying a grey level threshold. A 50x50 μm^2 square was used as a reference area to calculate the fibre volume fraction and was shifted along the carbon layer to calculate the local $V_{f,c}$. The glass fibre volume fraction was not possible to calculate accurately because the grey levels of the fibres were too similar to those of the matrix. We also tried to use the *circle detection function* in *MATLAB*, but the recognition rate of the glass fibres was unsatisfactory (i.e. lower that 50%) mainly due to random defects from sample polishing. The thickness of the carbon layer was estimated by measuring the length of a line drawn between the most external fibres of the layer at every 20 μm along the width of the analysed cross-section. We made 50 measurements in total for each image analysed.

3.4. Composite manufacturing

The hybrid composite configurations were made by sandwiching unidirectional IM7 carbon/913 epoxy, S-glass/913 epoxy and the interleaves together in a sequence symmetric to the mid-plane of the plate (Fig. 1). The baseline configuration was made with the same stacking sequence but excluding the interleaf layers. The 300x300 mm plates were cured in an OLMAR ATC 1100/2000 type autoclave at the curing temperature of 125 °C for 60 min and a pressure of 0.7 MPa, as recommended by the supplier of the prepregs. −950 mBar vacuum was applied after sealing the vacuum bag and in the initial part of the

Table 4
Results of the tensile tests on hybrid laminates (CoV in % expressed in brackets below the sample mean values, C-carbon/epoxy, G-glass/epoxy, EP-epoxy, numbers after the interleaf film material in the configuration designation mark the thickness in [μm], e.g. EP-30 – 30 μm epoxy film interleaved).

Material configuration	Measured thickness [mm]	Initial elastic modulus [GPa] calculated with		Knee-point stress [MPa] calculated with		Knee point strain[a] [%]	Mode II strain energy release rate [b] [kJ/m^2]	Estimated pseudo-yield strain [c] [%]
		nominal thickness (1.03 mm)	measured thickness	nominal thickness (1.03 mm)	measured thickness			
Baseline configuration – layup sequence [G_3/C/G_3]								
Baseline	1.081	60.3	57.3	1193.5	1132.7	1.95	2.043	
	(2.21)	(2.35)	(2.71)	(5.55)	(3.94)	(4.76)	(9.49)	
Film interleaved configurations – layup sequence [G_3/Film/C/Film/G_3]								
EP-30	1.130	60.0	54.3	1133.6	1025.4	1.89	1.919	0.669
	(2.41)	(5.59)	(4.61)	(4.02)	(2.37)	(4.98)	(9.84)	
EP-60	1.190	60.1	51.9	1199.9	1034.7.8	1.92	1.984	0.739
	(1.59)	(2.12)	(1.33)	(3.15)	(2.40)	(3.28)	(6.53)	(0.57)
ABS-30	1.131	59.4	54.0	1098.1	997.2	1.89	1.904	
	(2.20)	(3.61)	(2.27)	(5.45)	(3.65)	(3.33)	(6.68)	
ABS-60	1.192	59.6	51.3	1154.3	994.1	1.93	1.990	
	(2.27)	(4.00)	(2.62)	(5.24)	(4.75)	(2.59)	(5.21)	

[a] Determined according to Fig. 2. The strain values are not corrected for thermal residual strain, which is estimated to be 0.054% in the baseline configuration.
[b] G_{II} at the first fracture of the carbon layer according to equation (2.1).
[c] Calculated only for the samples that showed pseudo-ductile behaviour.

pressurisation phase in the autoclave. However, the vacuum was switched off after the pressure in the autoclave exceeded 1.2 bar. The samples were cut with a diamond cutting wheel. The nominal dimensions of the samples were 260x20x1.02 mm (nominal free length/width/thickness respectively). The interleaf films were inserted between the carbon and the glass layers (Fig. 1). Two thicknesses, 30 and 60 μm, were used for each film type. The thicker epoxy layer was fabricated by joining two 30 μm thick films. The ABS films were not wide enough to cover the 300x300 mm prepreg sheets, due to manufacturing related limitations. Then, two rectangular pieces of 150 mm width were placed side-by-side for each layer.

3.5. Evaluation of the mechanical parameters

The mechanical parameters of the hybrid composites, i.e. elastic modulus, knee-point stress and strain, pseudo-ductile strain, are defined in Fig. 2. The plots of the tensile stress-strain curves of all configurations as well as the mechanical parameters, were evaluated by using the nominal thickness of the baseline laminates, to make all configurations comparable to each other. In the interleaved configurations, the thickness of the interleaves was not considered when calculating the stress in the laminate as their elastic moduli are more than one order of magnitude lower than that of the fibre-reinforced layers. However, the interleaf layers affect the weight and the full thickness of the laminate to some extent, and therefore should be taken into account when a structure is designed. For completeness, Table 4 also includes the knee-point stress and the initial elastic modulus calculated with the actual thickness of the interleaved laminates, to make the comparison of the same parameters calculated with different thicknesses possible. We introduced the parameter Δσ to evaluate the intensity of the stress drops subsequent to the sudden spread of delamination in the samples. Δσ is expressed as the average of the first major stress drop exhibited by the samples. The samples which failed in a pseudo-ductile way, i.e. in the absence of any stress-drops, were considered with the value of zero in the calculation of

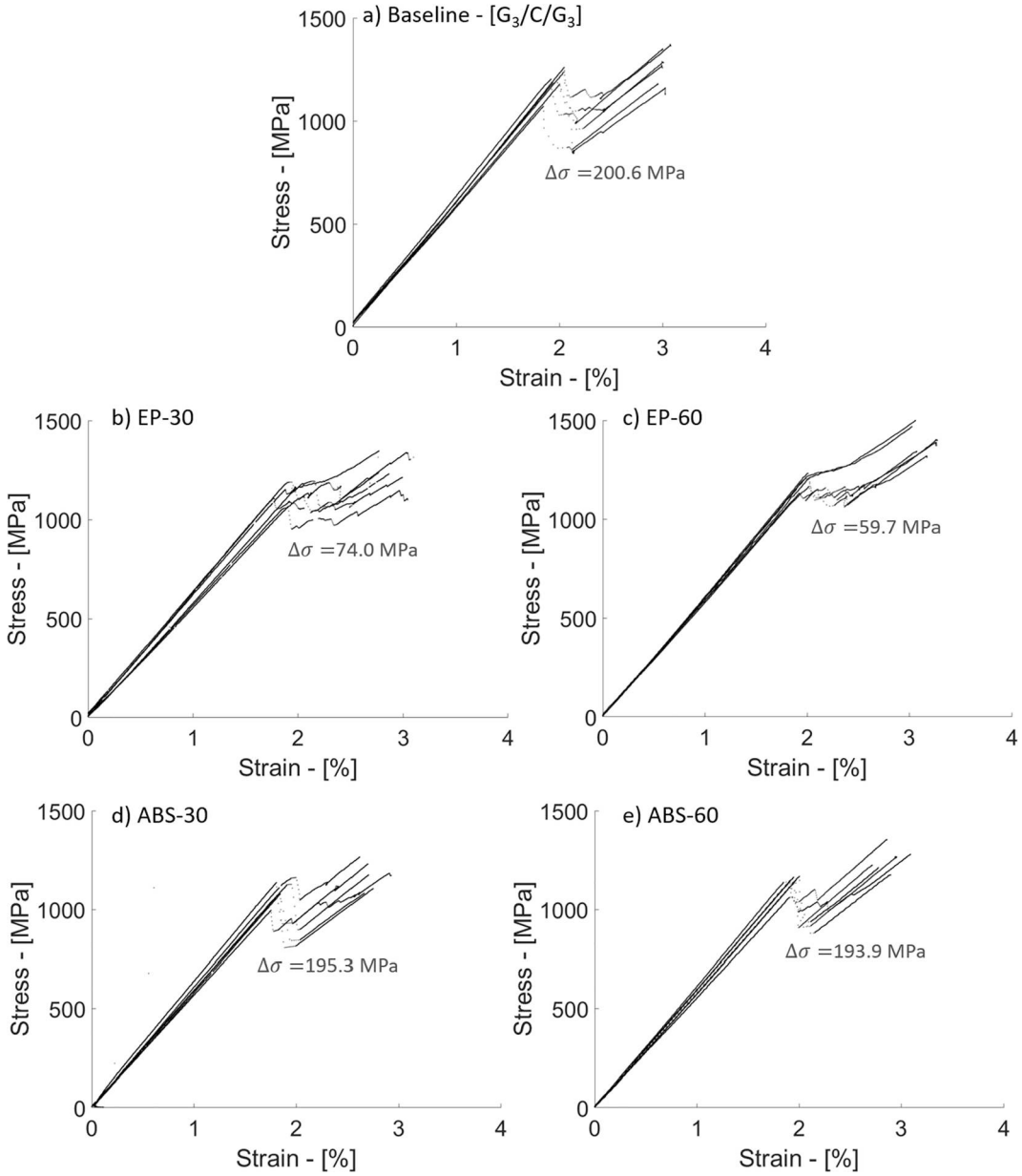

Fig. 4. Stress-strain curves of tensile tests on the baseline and interleaved configurations. The plots also report the average Δσ of the first drops at delamination after the fracture of the carbon layer (the coefficient of variation in percentage - CV% - is expressed below the mean value). (For interpretation of the references to colour in this figure legend, the reader is referred to the web version of this article.)

Δσ. Δσ is reported in the figure of the tensile stress-strain curves (see Fig. 4).

4. Results and discussion

4.1. Baseline configuration

The stress-strain curves related to the baseline configuration are reported in Fig. 4(a). The damage modes in the samples of the baseline configuration (i.e. [G_3/C/G_3]) mostly matched the predictions of the damage mode map in Fig. 3(b). The tested samples exhibited catastrophic delamination, triggered by the fracture of the carbon/epoxy layer. Typically, the carbon layer exhibited a single full-width fracture in the sample (see Fig. 5(a)). The full-width fracture caused the sudden delamination that usually spread along the full specimen area or covered a large portion (roughly 70%) of the sample surface and continued to propagate upon further strain increase. The delamination caused stress drops in the tensile stress-strain curves. The stress drops marked the end of the initial linear stage of the tensile stress-strain response and were characterised by a loss of the carbon layer contribution to the tensile modulus of the hybrid laminate (see Fig. 5(b)).

Three out of six baseline specimens exhibited mixed damage mode characterised by delamination and fragmented regions (with multiple fractures of the carbon layer) limited to stripes typically narrower than one third of the full specimen width (see Fig. 5(b.4)). According to the videos recorded by the optical strain measurement system, these long and narrow fragmented regions formed suddenly, together with the initial delamination (up to half of the full free length), therefore we need to distinguish them from the progressive fragmentation (one-by-one fracturing) of the LSM layer observed earlier in thin-ply hybrids [5]. Further propagation of delamination and fragmentation was stable. The sudden arising of the fragmented stripes suggests two things: (1) The carbon/epoxy prepreg ply may have different properties (most probably thickness) due to manufacturing variations in the fragmented zone and release slightly less energy upon the first overall fracture of the layer. (2) Dynamic effects should have played an important role as fragmentation along the full specimen happened at once, not progressively. Further analysis of the architecture of our laminates is given below, but analysis of the possible dynamic effects does not belong to the scope of this study and deserves attention in the future. Nevertheless, a key indication of the observed mixed damage mode of the baseline configuration in our present study is, that the baseline configuration is already near the borderline between *catastrophic* delamination and fragmentation + dispersed delamination on the damage mode map (Fig. 3 (b)). Improvement of the G_{IIC} of the hybrid laminates is likely to promote the total fragmentation of the carbon layer with diffused, progressive

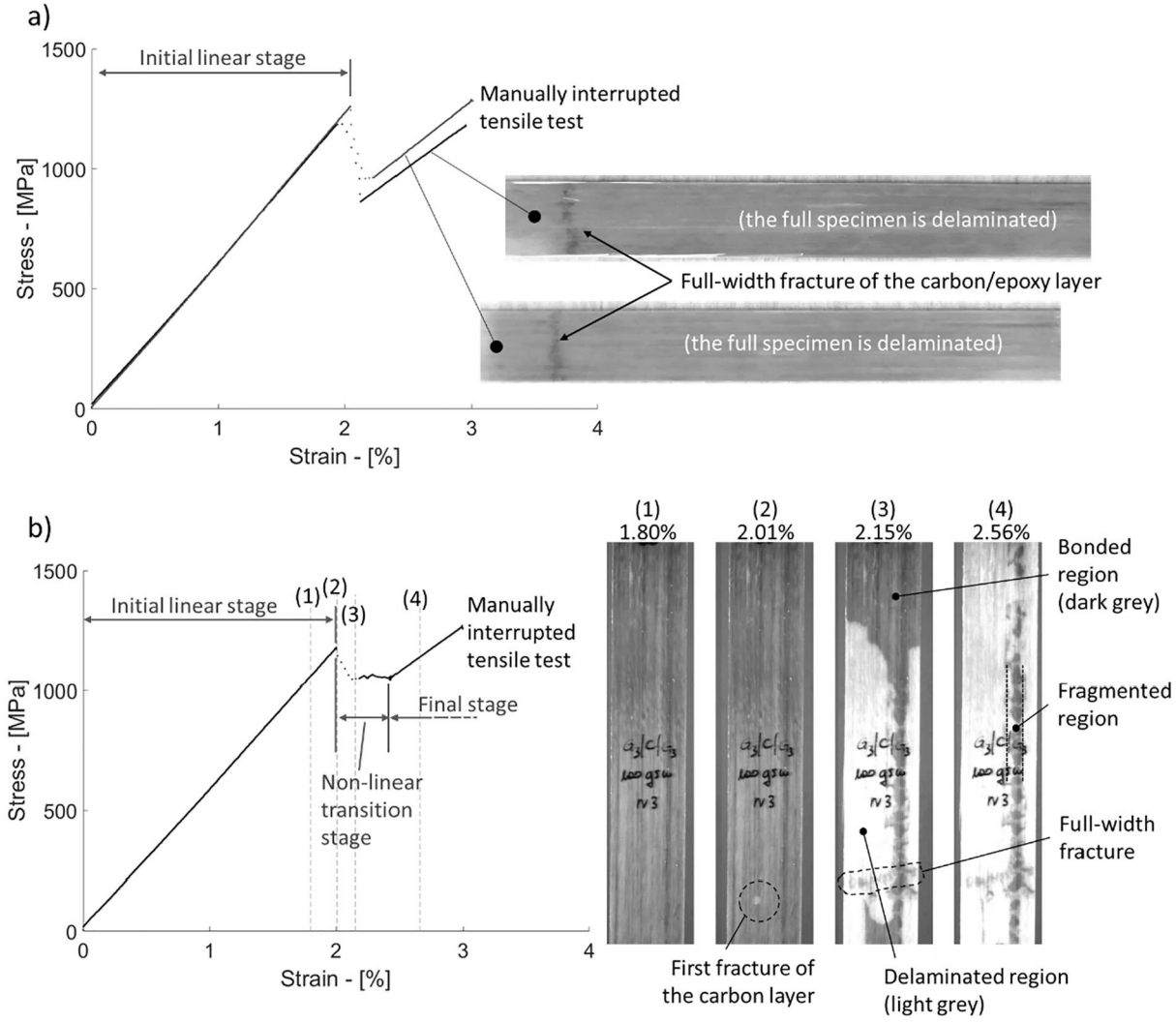

Fig. 5. Stages of damage propagation in the continuous unidirectional G_3/C/G_3 (baseline) samples during the tensile test. (a) Shows two samples catastrophically delaminated after a full-width fracture of the carbon layer. (b) Shows a sample which have shown mixed fragmentation and delamination. (For interpretation of the references to colour in this figure legend, the reader is referred to the web version of this article.)

delamination.

One of the partially fragmented samples is examined in detail in Fig. 5(b). The first fracture of the carbon layer occurred in the gauge region at 2.01% strain (Fig. 5(b.2)). The fracture was initially small (about 1 mm wide) in the carbon layer. Then, it extended suddenly to the full width of the sample (see Fig. 5(b.3)) and triggered delamination between the carbon and the glass layers in up to half of the specimen area. The sudden delamination generated a stress drop between the stages (b.2) and (b.3). The delaminated area (lighter grey) is well visible from the outer surface of the samples, due to the translucency of the outer glass/epoxy composite layer [54]. Images (b.3) and (b.4) of Fig. 5 show the partially and fully delaminated sample, respectively. The fragmented region is distinguishable by the contrast between the delaminated (light grey) and still bonded (dark grey) parts. At stage (b.4), the delaminated carbon layer no longer contributed to the load bearing capacity of the sample, then the stress-strain curve rose again linearly with a reduced slope.

The reasons for parallel development of fragmented parts and unstable delamination were investigated, and shown in Fig. 6, by analysing subsequent cross-sections of the sample presented in Fig. 5(b). The parts related to the fragmented region consistently showed lower carbon/epoxy layer thickness compared to that of the delaminated zones. The cross-sectional analysis in Fig. 6 shows a thicker section of the carbon layer (92 μm) in the delaminated part (see image (d)) and a thinner one (only 54 μm) in the fragmented zone (see image (e)). The varying thickness may have been caused by non-uniform layer thickness formed during prepreg manufacturing. The lower ply thickness implies a less stiff carbon layer that consequently releases lower energy at its first fracture. The transition zones between fragmented and delaminated areas are characterised by fractures in the carbon/epoxy layer (see Fig. 6 (a, c and e)) possibly originated from delamination and arrested in the central layer as the driving forces became non-uniform towards the fragmented zones. Three cross-sections from the region where the first fracture of the carbon layer occurred was analysed in detail in Fig. 6. The full width fracture zone of the carbon layer is shown in image (b), and it is the point where the delamination cracks originated from and caused the large-scale delamination of the carbon and the glass layers.

The average strain to failure of the carbon layer registered experimentally was 1.95% (see Table 4), higher than the value in the supplier's datasheet (1.68%) for UD composite specimens (see Table 2). The obtained carbon layer failure strain is even higher than the 1.90% quoted for dry fibres by the manufacturer (see Table 1). A higher strain to failure of the carbon/epoxy layer is expected due to the protective effect of the glass layers that cover the carbon layer and eliminate the stress concentration at the edge of the gripping area [48,55,56]. An extra increment may be given by the thermal residual strain generated during the cool down phase of the curing cycle of the laminates, which is estimated to be 0.054% for this material configuration. After the correction for the thermal residual strain, the failure strain of the carbon/epoxy layer agrees well with the carbon fibre failure strain. UD carbon/epoxy tensile failure strains very close to fibre failure strains were observed earlier as well in [57].

4.2. Epoxy film interleaved hybrid laminates

The tensile tests performed on epoxy film interleaved laminates showed significant changes in the damage modes in contrast to the baseline configuration. For simplicity, we will refer to the 30 and 60 μm

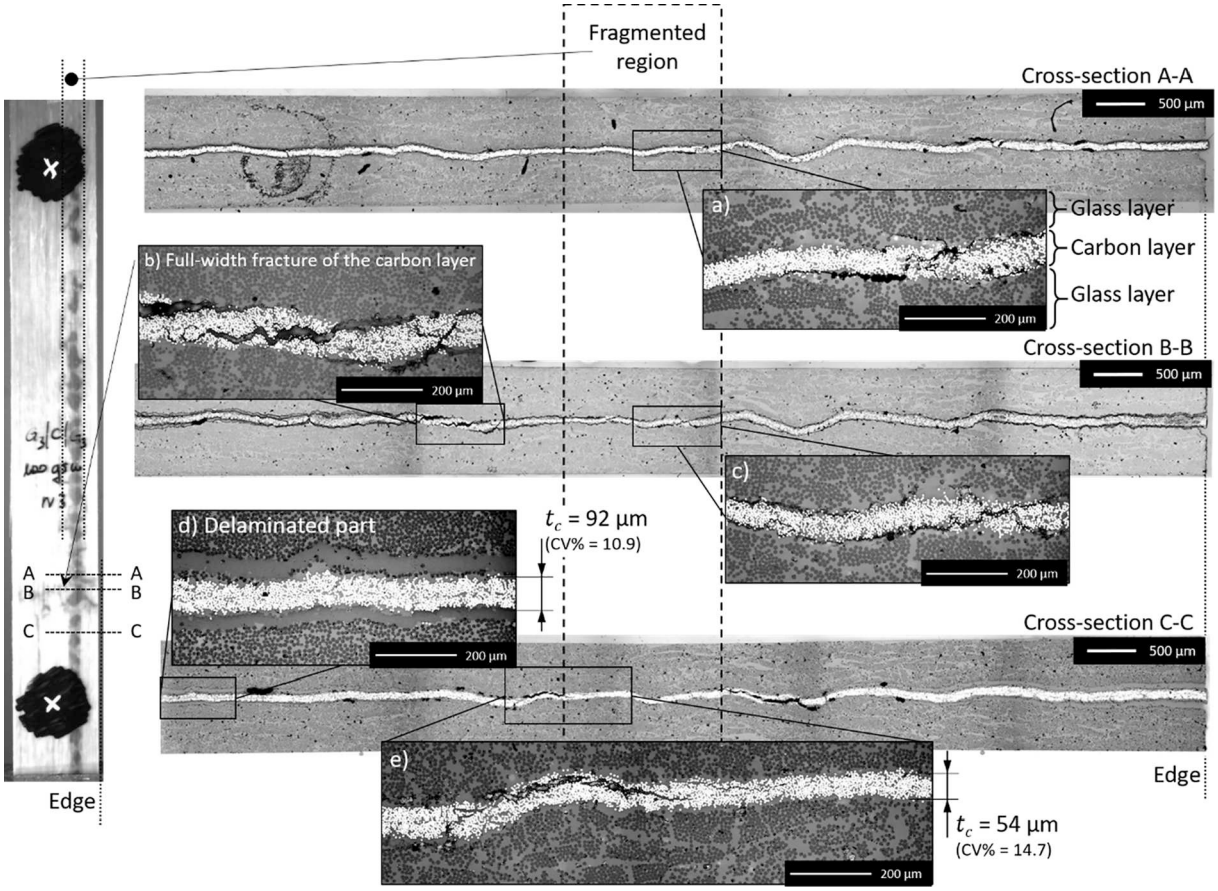

Fig. 6. Cross-sectional optical microscopy analysis of a sample from the baseline series which showed fragmentation and delamination. There are three cross-sections from the region from which the damage initiated and then propagated towards the rest of the sample. (For interpretation of the references to colour in this figure legend, the reader is referred to the web version of this article.)

epoxy film interleaved configurations as EP-30 and EP-60, respectively. Fig. 4(b) and (c) show that the average intensity of the stress drops (i.e. $\Delta\sigma$) caused by sudden delamination decreased with the thickness of the epoxy films, and the coefficients of variation of the stress before the first load-drop (see knee-point stress in Table 4) was slightly decreased, indicating more stable and slightly more consistent failure mode than that of the baseline series. The majority of the epoxy interleaved samples (5 out of 6 for EP-30 and 4 out of 6 for EP-60) exhibited higher delamination resistance than that of the baseline ones resulting in a mixture of carbon/epoxy layer fragmentation limited to about one third of the specimen width and delamination in the rest developing in parallel (see Fig. 7(a, b)). An initial delamination of variable area occurred after the first full-width fracture of the LSM layer and it was followed by several further, limited delaminations generating multiple stress drops with reduced $\Delta\sigma$ in the plateau stages of the stress–strain curves. The extent of the first stress drop of each specimen was reduced significantly (from 200 MPa for the baseline to 74 MPa (EP-30) and 59 MPa (EP-60) in average) which indicates an increased G_{IIC}. In both epoxy film interleaved configurations (i.e. EP-30 and EP-60), the areas covered by initial sudden delamination, were significantly smaller than those of the baseline configuration as well (see Fig. 7 (a, b)). One out of six samples of the EP-30 series and two out of six of the EP-60 samples showed a pseudo-ductile behaviour, with full fragmentation of their carbon/epoxy layer, generating a stable, rising plateau without any stress-drops in the stress-strain curves, reported in Fig. 8. Here, there were multiple full width fractures of the carbon layer that progressively covered the free lengths of the samples. The delaminated areas around the carbon layer fractures were small and diffused along the samples, as it is visible in Fig. 8. The observed changes in the damage modes compared to the baseline configurations point towards more pseudo-ductile failure processes. Since the energy release rate of all tested configurations are similar (within the experimental scatter in Table 4) due to similar layer stiffnesses, the observed changes in the failure mode indicate an increase in the G_{IIC} of the epoxy interleaved configurations.

The knee-point strain of the pseudo-ductile samples was 2% for both configurations. For completeness, the pseudo-ductile strain (ε_{pd}) of these samples was also evaluated. It was 0.67% for the EP-30 sample, and 0.74% in average for the two EP-60 samples. As all the tensile tests were interrupted before the final failure of the samples, ε_{pd} was estimated by extending the stress-strain curves beyond the termination point up to the supposed strain to failure of the glass layers (Fig. 8). The strain to failure of the glass fibres considered here is estimated from previous results on similar S-glass/epoxy composites, i.e. 3.7% [5].

We investigated the differences in the damage modes between the baseline and the epoxy interleaved configurations by scanning electron microscope analysis. The SEM images in Fig. 9 compare the delaminated surfaces of the three configurations, showing similar surface morphology and damage patterns, i.e. hackled epoxy resin "channels" between fibres typical for shear deformations. These images do not show zones of higher resin content in the interleaved configurations explicitly, as could be expected due to extra matrix material inserted locally to the layer interfaces. Instead, the cross-sectional analysis in part a), b) and c) of Fig. 10, made on pristine samples, clearly show increased presence of epoxy at the layer interfaces together with a progressive decrease of the fibre volume fractions and increase of carbon/epoxy layer thickness in the epoxy film interleaved configurations with interleaf thickness. It indicates that part of the extra epoxy from the interleaf layers migrated into the neighbouring fibre reinforced layers during the curing process at elevated temperatures, when the viscosity of the matrix dropped, and flow was enabled. The insets in images a), b) and c) of Fig. 10 also clearly show a decrease in the fibre volume fraction at the carbon/glass layer interfaces. In fact, the carbon fibre volume fraction ($V_{f,c}$) was significantly decreased in the epoxy film interleaved configurations compared to that of the baseline (see Fig. 11).

The post-mortem analysis of the baseline and epoxy interleaved configurations provided useful information on the delamination and fragmentation in hybrid composites. The damage initiation in hybrid composites initiated with carbon/epoxy layer fracture when the carbon fibres reached their failure strain (see stage 1 Fig. 10). The fracture of the carbon layer released a given amount of energy (i.e. G_{II}) causing a given amount of delamination of the carbon and the glass layers depending on the G_{IIC} of the layer interface. The cross-section analysis made on

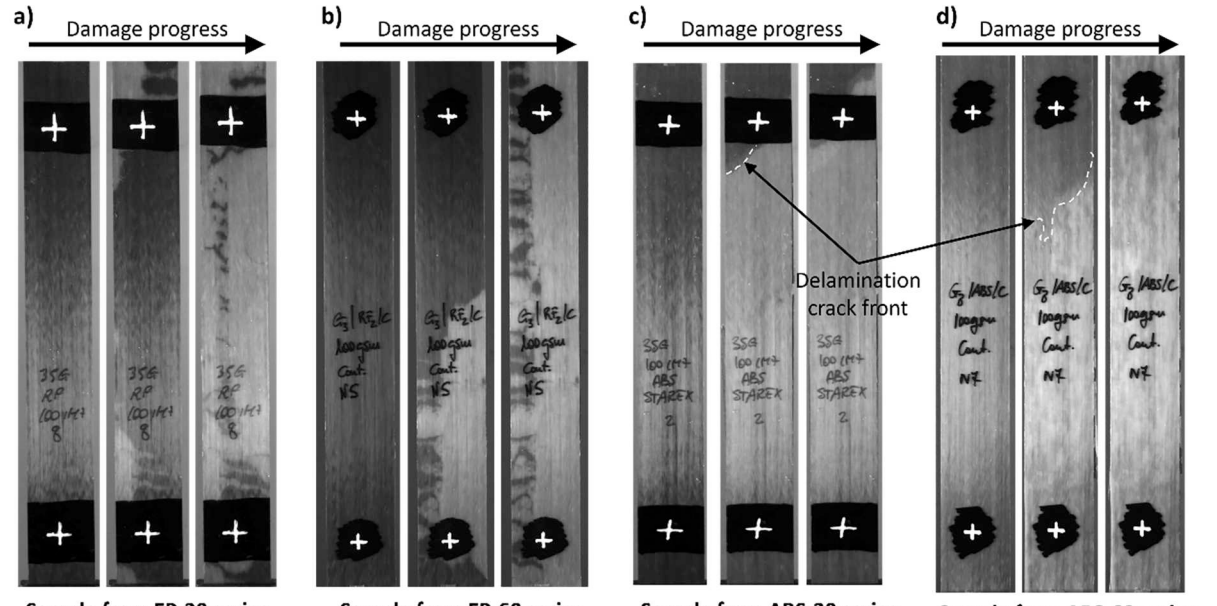

Fig. 7. Typical damage modes of the interleaved hybrid composite configurations.

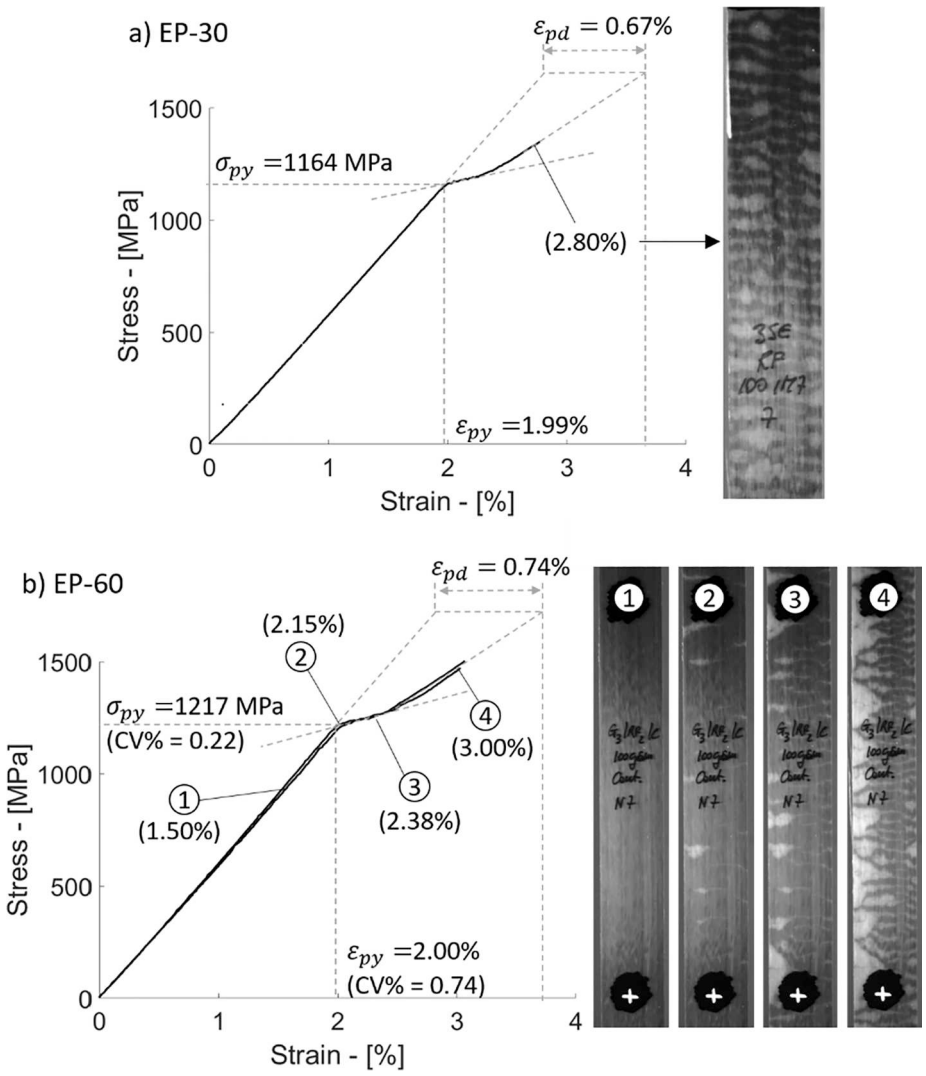

Fig. 8. Pseudo-ductile stress-strain curves of one 30 μm (EP-30) and one typical 60 μm epoxy film (EP-60) interleaved samples. The images correspond to the damage stages indicated on the stress-strain curves. (For interpretation of the references to colour in this figure legend, the reader is referred to the web version of this article.)

delaminated samples revealed that the mode II fracture propagation typically happened inside the glass/epoxy layers close to the layer interface. In fact, some glass fibres usually stayed attached to the delaminated carbon/epoxy layer (see stage 2 (e) and (f) in Fig. 10).

The samples that showed partial or full fragmentation during the tensile tests were characterised by multiple fractures of the carbon layer, diffused along the sample. The damage process was progressive with several small amounts of energy released. The cross-section analysis of the fragmented samples showed that the translaminar cracks, generated by the fracture of the carbon/epoxy layer, were arrested at the interface between the carbon/epoxy and glass/epoxy layers and did not propagate in the edge of the glass/epoxy layer as in the baseline case (compare images (g) and (f) of Fig. 10). The propagation of mode II delamination cracks in the matrix of FRPCs is widely studied in literature, for example in [58–61], and the crack propagation is governed by shear yielding of matrix and fibre/matrix debonding.

The interfaces modified by epoxy films provided higher volume fraction of the matrix material which resulted in a structure where larger volume of epoxy resin had to be fractured to separate the glass and carbon fibre reinforced layers, therefore the epoxy interleaved samples showed higher interlaminar fracture toughness than the baseline ones.

4.3. ABS film interleaved hybrid composites

The configurations interleaved with ABS films showed damage modes characterised by catastrophic delamination after the first fracture of the carbon/epoxy layer (Fig. 7(c, d)). Typically, the delamination was triggered by a full-width fracture of the carbon layer and generated sudden stress drop in the stress-strain graphs (Fig. 4(d, e)). The decrease of Δσ associated with the stress drops was negligible for these configurations in comparison to the baseline (Fig. 4(d, e)).

The negligible effect of ABS films on hindering the sudden spread of delamination after the fracture of the carbon/epoxy layer and the stress-strain curves similar to those of the baseline specimens indicated that this interleaf material was ineffective in toughening the interfaces of the hybrid laminates. No sign of fragmentation was observed during the tensile tests, which suggests that the ABS film interleaved layer interfaces were even weaker than those of the baseline specimens. Nevertheless, the microscopy analysis (see Figs. 12 and 13) enabled insight into the structure of the laminates and the bonding between the fibre reinforced layers and the ABS interleaves.

In both configurations, the optical micrographs of the cross-sectional samples revealed a 2–3 glass fibres thick layer of the epoxy matrix composite blocks partially impregnated by ABS (see the insets of Fig. 12 (a) and (d)), based on the colours of the resins (ABS–white,

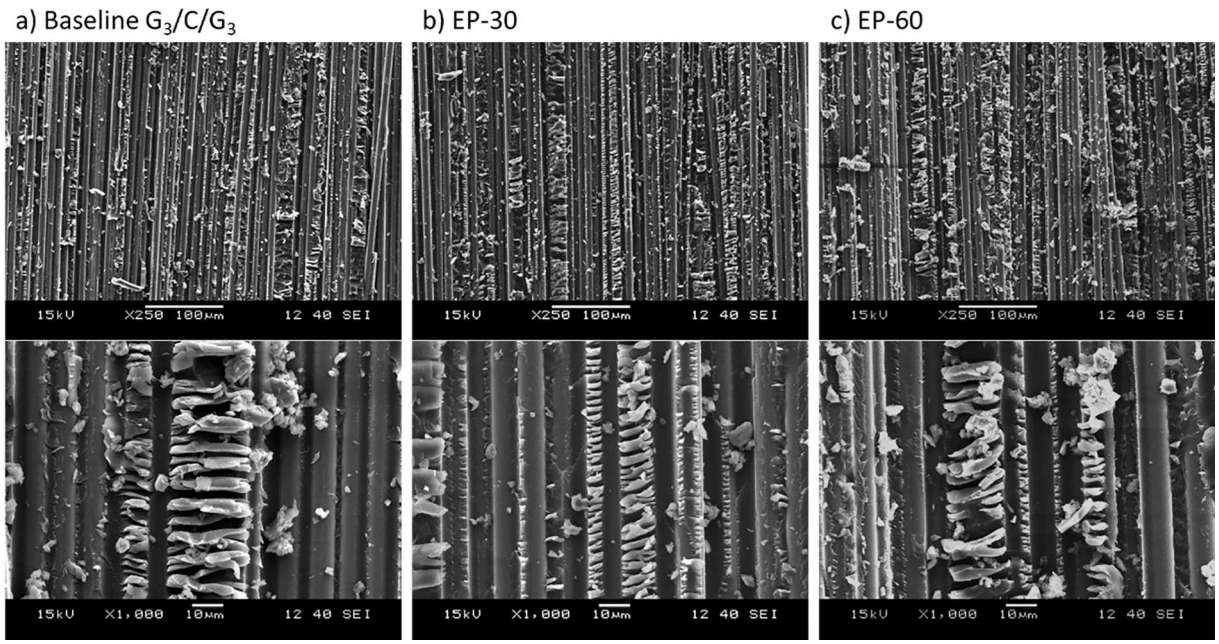

Fig. 9. SEM analysis of the fractured layer interfaces of (a) the baseline configuration $G_3/C/G_3$ and of the 30 μm (b) and 60 μm (c) epoxy film interleaved hybrid laminates. All the images show the carbon layer side of the fractured interfaces. (For interpretation of the references to colour in this figure legend, the reader is referred to the web version of this article.)

epoxy–orange). The penetration of ABS into the epoxy matrix of the composite plies embedded some fibres as well, but the different materials still formed separate phases with clear boundaries (see the insets of Fig. 12(a) and (b)). The ABS penetration into the carbon layer was not as deep as in the glass layers, probably due to the different fibre volume fraction of the two layers, which was 48% for the glass and 58% for the carbon reinforced one (see Table 2). The less dense packing of glass fibres may have enabled deeper penetration of the ABS into this layer during the crosslinking process of the hybrid laminates, at temperatures higher than the glass transition temperature (T_g) of ABS, i.e. 104 °C. The conditions for the penetration at the epoxy matrix composite-ABS film interfaces were fulfilled during the final part of the temperature ramp and the initial period of the crosslinking stage of the cure cycle in the autoclave above 80 °C and then at 125 °C. In this temperature range the viscosity of the epoxy dropped significantly (from 80 °C), but crosslinking had not yet approached the gel phase, while the ABS softened (from 100 °C) above its T_g. The 0.7 MPa pressure applied in the autoclave during the curing process could have promoted the ABS penetration into the fibre-reinforced layers until the epoxy matrix reached gel and then solid phase. The penetration of ABS into the composite layers generated an inter-locking structure at the interfaces, which led to strong bonding at the composite-interleaf interface and governed the damage mechanisms and corresponding patterns observed in the SEM images of Fig. 13, and the cross-section images in Fig. 12.

The ABS film thicknesses affected the resulting appearance of the surface after delamination (see Fig. 13). In the ABS-30 samples, both sides of the delaminated surfaces exhibited similar texture showing that the ABS damaged in shear was fully covering the fibre-reinforced layers (Fig. 13(a, b)). The absence of fibre debonding, which was the dominant feature in the baseline specimens (see Fig. 9), indicated that delamination propagated within the ABS layers and not at the interface between the composite layer and the ABS film. This hypothesis is also supported by the cross-sectional analysis of the ABS-30 series, which show continuous layers of ABS films still attached to the delaminated fibre reinforced/epoxy layers (see Fig. 12(b)).

The delamination in the ABS-60 series was characterised by thick blocks of ABS with a smoother texture attached to one of the neighbouring composite layers, as shown in Fig. 13(c). Images (c) and (d) of Fig. 13 show the same spot on the carbon/glass interface from the carbon side and the glass side. The magnified regions capture the deviation of the delamination crack towards one to the other composite layer within the ABS film. The longitudinal- and the cross-section images of the ABS-60 samples (see Fig. 12(e, f)) revealed that these deviations of the crack in the ABS layer were frequent and formed a zig-zag route. The several deviations of the crack may have induced significant mode I stress components besides the mode II loading and made the overall fracture character of the thicker ABS layer less ductile, as indicated by the smoother fracture surfaces observed on the SEM images of Fig. 13 (c) and (d). The smoother fracture surface of the ABS-60 sample is more typical of mode I separation, while the detailed fracture surface fully covered by highly stretched and broken ligaments observed in the ABS-30 sample corresponds to more ductile, shear dominated failure. These observations support the hypothesis, that the mode I stress component was increased significantly in the ABS-60 specimens with thick interleaves. The crack deviation mechanism was observed only in the thick ABS films, as the 30 μm film in the other configuration was probably too thin for the formation of ABS blocks.

Unlike the baseline configuration, delamination did not migrate into the glass/epoxy layers of the ABS interleaved hybrid laminates. The continuous ABS layers protected the glass/epoxy layers from the penetration of the delamination cracks, which instead propagated only within the ABS films. Since the bonding between the composite and the ABS layers was excellent (due to the interlocking structure), delamination propagation was governed by the shear strength and fracture toughness of the ABS films. The ABS films acted as barriers between the glass/epoxy and carbon/epoxy layers and prevented the epoxy migration between them. In fact, the carbon fibre volume fraction of both ABS interleaved configurations, was similar to that of the baseline configuration (see Fig. 11). Based on the micrographs the bonding between the composite layers and the ABS interleaves was excellent, therefore the absence of any toughening effect is attributed to the subcritical shear properties of the ABS films. A possible future task is to find new interleaf materials with similarly good bonding to the composite layers, but with superior shear properties.

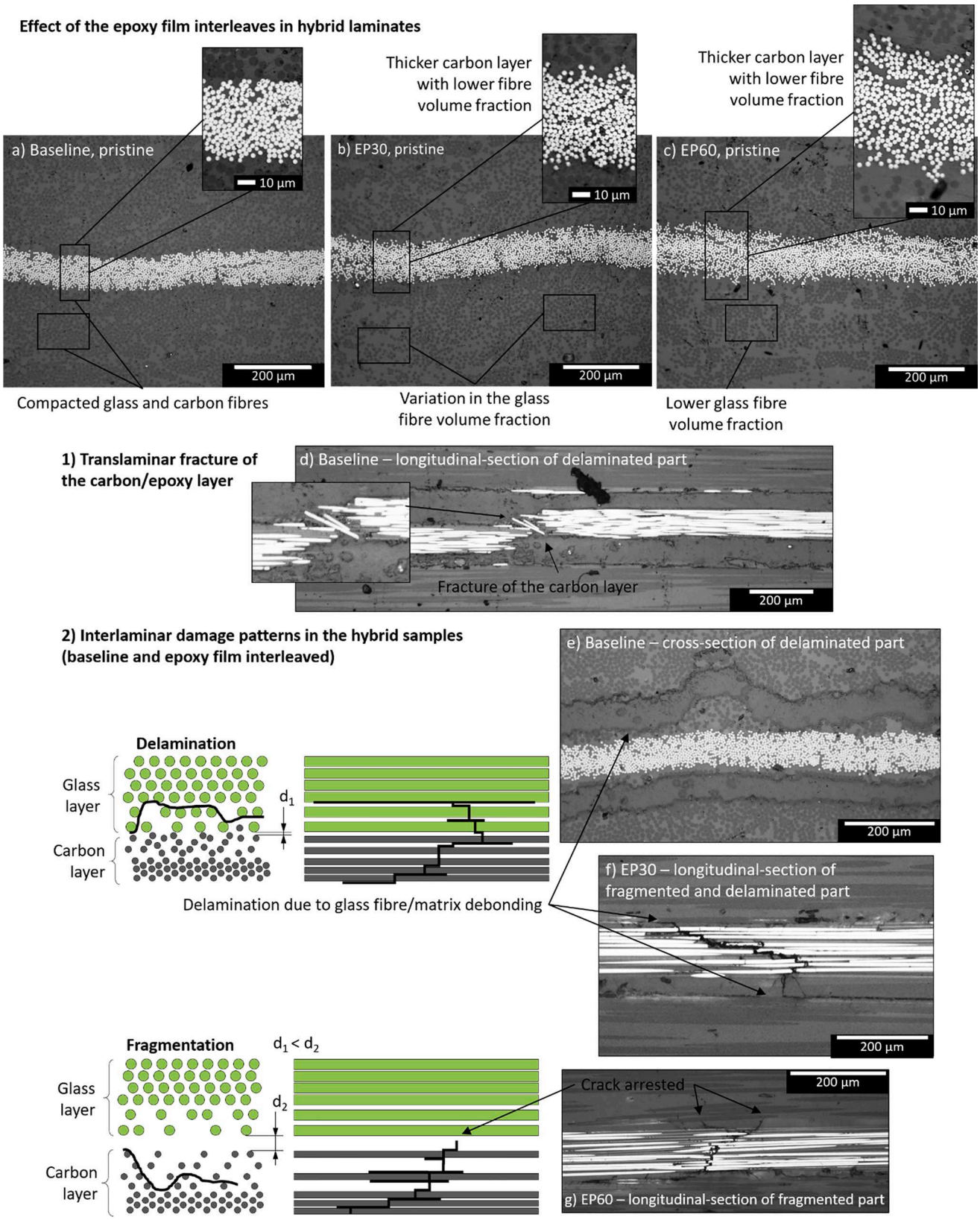

Fig. 10. Cross-section analysis of the pristine and tested epoxy film interleaved samples, conducted with an optical microscope, and stages of the damage progress in the layers of the hybrid composites. (For interpretation of the references to colour in this figure legend, the reader is referred to the web version of this article.)

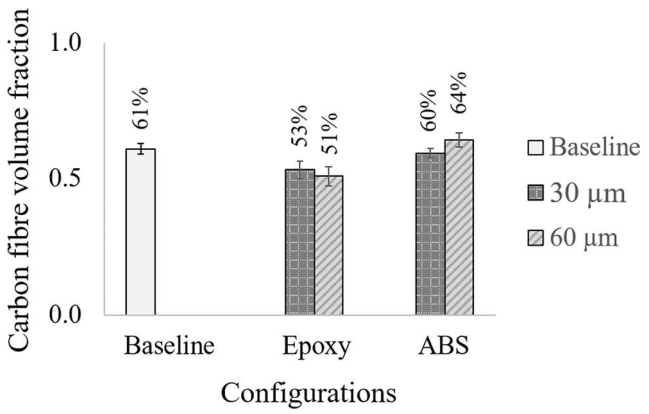

Fig. 11. Carbon fibre volume fraction ($V_{f,c}$) in the baseline and film interleaved hybrid laminates. (For interpretation of the references to colour in this figure legend, the reader is referred to the web version of this article.)

5. Conclusions

We evaluated the possibility of achieving pseudo-ductility in carbon/glass-epoxy interlayer hybrid composites made of standard thickness carbon/epoxy and glass/epoxy plies interleaved with epoxy and ABS films. The baseline configuration (i.e. without interleaves) failed catastrophically, with delamination between the carbon and the glass layers typically triggered by full-width fractures of the carbon layer. Three out of six samples of the baseline series exhibited small regions characterised by fragmentation (i.e. multiple fractures of the carbon/epoxy layer). The cross-section analysis revealed a lower thickness of the carbon/epoxy layer in the fragmented regions than that observed in the delaminated zones. The local variations in the carbon layer thickness influenced the damage mode as the fracture of a locally thinner carbon layer did not release enough energy to delaminate the fibre reinforced layers completely.

The epoxy film interleaved hybrid composites showed damage modes characterised by full fragmentation of the carbon layer or mixed damage patterns with delaminated and fragmented parts. Pseudo-ductility was observed in the fully fragmented samples, with a pseudo-ductile strain of 0.67% for the EP-30 configuration and 0.74% for EP-60. The stress-strain curves had a stable, rising plateau due to the full fragmentation of the carbon/epoxy layer. The pseudo-ductile epoxy interleaved samples showed multiple, typically full-width fractures with only local delamination around them resulting in a dispersed energy release pattern. The absence of sudden and extensive spread of delamination at the first carbon/epoxy layer fracture observed in the baseline samples indicated an increase in G_{IIC}. The epoxy film interleaves significantly reduced the carbon fibre volume fraction (−12.7 rel.% and −16.5 rel.% in EP-30 and EP-60, respectively) in the hybrid laminate. This resulted in higher delamination resistance by an increase in the volume of the matrix material to be fractured to separate the composite layers. This favourable change in the damage mode was associated with the higher energy level (G_{IIC}) required to fracture an interface with a larger amount of epoxy between the fibres.

The ABS film interleaving was ineffective in the hybrid laminates for preventing catastrophic delamination. The bonding between ABS and the fibre-reinforced layers was characterised by a phase-separated inter-locking ABS/epoxy structure formed during the curing process of the hybrid composite laminates. The inter-locking structure contributed to effectively transfer the shear deformation into the ABS layers from the fibre-reinforced layers. The delamination propagated within the ABS layer only, and the glass/epoxy layers were protected from the penetration of translaminar cracks originated from the carbon/epoxy layer fractures. Higher efficiency in suppressing delamination may be

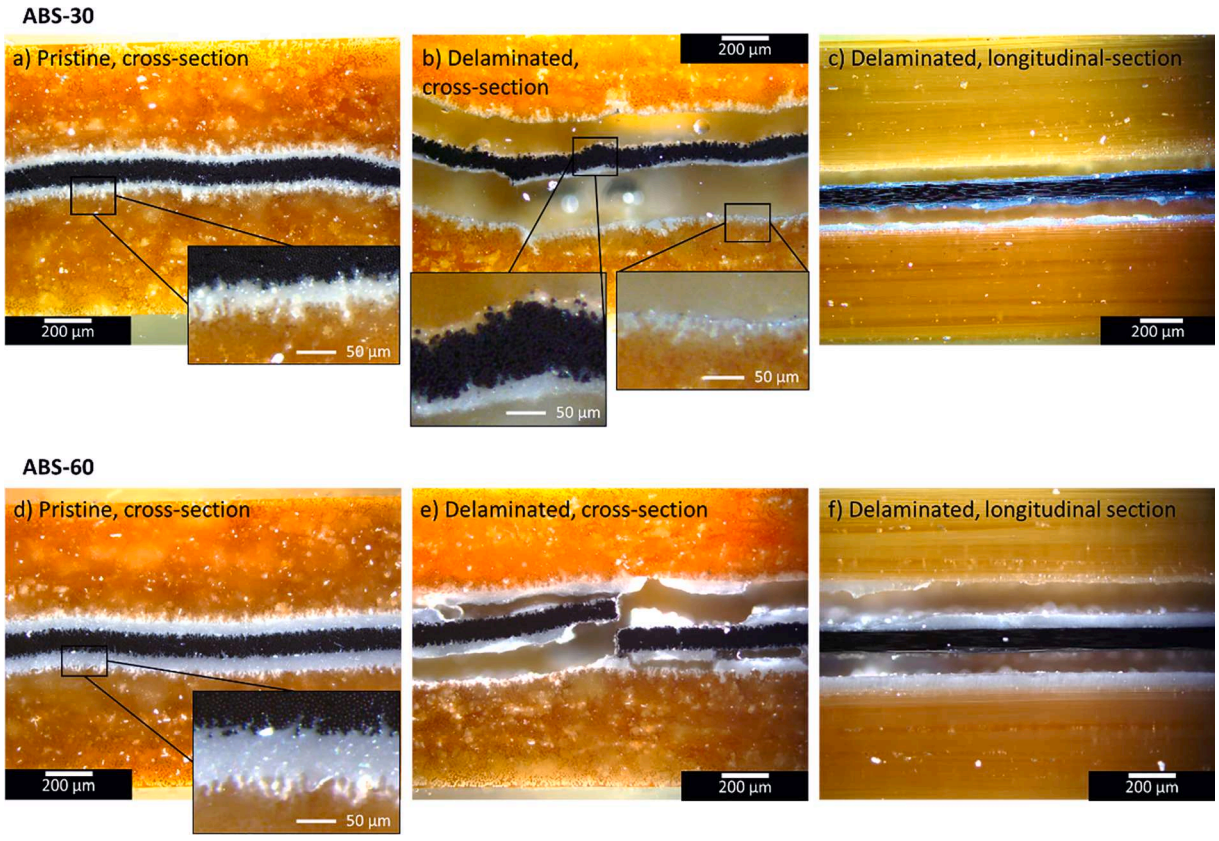

Fig. 12. Cross-section analysis of the pristine and tested ABS film interleaved samples, conducted with an optical microscope in dark field mode. (For interpretation of the references to colour in this figure legend, the reader is referred to the web version of this article.)

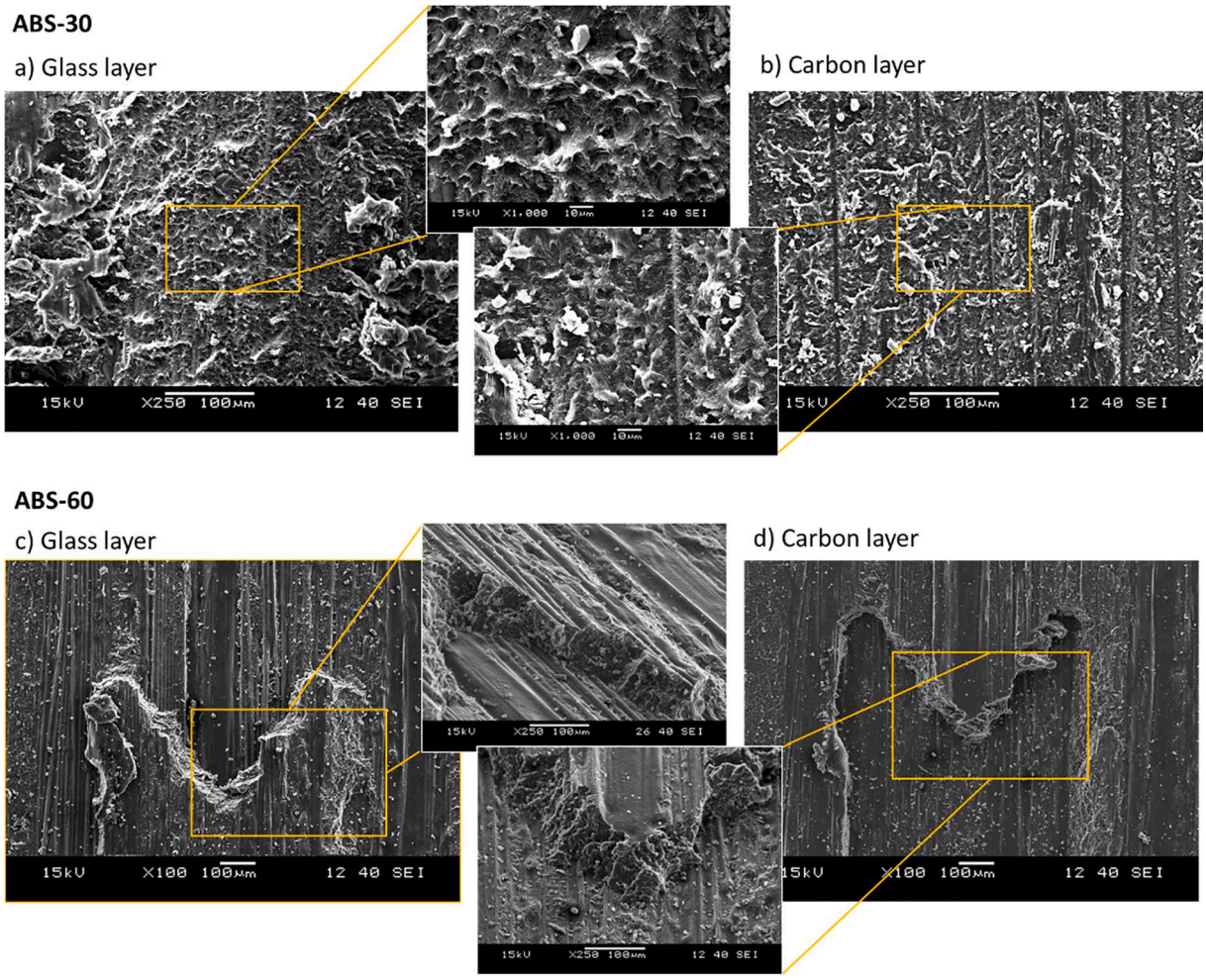

Fig. 13. SEM analysis of the fractured (a) glass and (b) carbon layers. (For interpretation of the references to colour in this figure legend, the reader is referred to the web version of this article.)

obtained using thermoplastic layers with higher shear strength and toughness than that of the applied ABS.

The results indicate that the interleaving technique can be considered as a possible route to achieving the desired pseudo-ductility in unidirectional continuous fibre hybrid composites, which originally showed unstable damage modes.

CRediT authorship contribution statement

Salvatore Giacomo Marino: Conceptualization, Methodology, Formal analysis, Investigation, Writing - original draft. **Gergely Czél:** Conceptualization, Methodology, Resources, Writing - review & editing, Supervision, Project administration, Funding acquisition.

Declaration of Competing Interest

The authors declare that they have no known competing financial interests or personal relationships that could have appeared to influence the work reported in this paper.

Acknowledgements

The research leading to these results has been performed within the framework of the *HyFiSyn* project and has received funding from the European Union's Horizon 2020 research and innovation programme under the *Marie Skłodowska-Curie* grant agreement No 765881. The research reported in this paper and carried out at BME was also supported by the National Research, Development and Innovation Office (NRDI, Hungary) through grants OTKA FK 131882 and TKP2020 IES, Grant No. BME-IE-NAT the latter based on the charter of bolster issued by the NRDI Office under the auspices of the Ministry for Innovation and Technology (Hungary). Gergely Czél is grateful for funding through the Premium Postdoctoral Fellowship Programme of the Hungarian Academy of Sciences.

References

[1] Czél G, Wisnom MR. Demonstration of pseudo-ductility in high performance glass/epoxy composites by hybridisation with thin-ply carbon prepreg. Compos Part A Appl Sci Manuf 2013;52:23–30. https://doi.org/10.1016/j.compositesa.2013.04.006.

[2] Jalalvand M, Czél G, Wisnom MR. Parametric study of failure mechanisms and optimal configurations of pseudo-ductile thin-ply UD hybrid composites. Compos Part A Appl Sci Manuf 2015;74:123–31. https://doi.org/10.1016/j.compositesa.2015.04.001.

[3] Czél G, Jalalvand M, Wisnom MR, Czigány T. Design and characterisation of high performance, pseudo-ductile all-carbon/epoxy unidirectional hybrid composites. Compos Part B Eng 2017;111:348–56. https://doi.org/10.1016/j.compositesb.2016.11.049.

[4] Wisnom MR. Mechanisms to create high performance pseudo-ductile composites. In: IOP Conf. Ser. Mater. Sci. Eng., vol. 139; 2016. https://doi.org/10.1088/1757-899X/139/1/012010.

[5] Czél G, Jalalvand M, Wisnom MR. Design and characterisation of advanced pseudo-ductile unidirectional thin-ply carbon/epoxy-glass/epoxy hybrid composites. Compos Struct 2016;143:362–70. https://doi.org/10.1016/j.compstruct.2016.02.010.

[6] Czél G, Jalalvand M, Wisnom MR. Demonstration of pseudo-ductility in unidirectional hybrid composites made of discontinuous carbon/epoxy and continuous glass/epoxy plies. Compos Part A Appl Sci Manuf 2015;72:75–84. https://doi.org/10.1016/j.compositesa.2015.01.019.

[7] Czél G, Pimenta S, Wisnom MR, Robinson P. Demonstration of pseudo-ductility in unidirectional discontinuous carbon fibre/epoxy prepreg composites. Compos Sci Technol 2015;106:110–9. https://doi.org/10.1016/j.compscitech.2014.10.022.

[8] Bismarck A, Bacarreza O, Blaker J, Diao H, Grail G, Pimenta S, et al. Exploring routes to create high performance pseudo-ductile fibre reinforced composites. In: ICCM Int. Conf. Compos. Mater., vol. 2015- July, Copenhagen; 2015.

[9] Finley JM, Yu H, Longana ML, Pimenta S, Shaffer MSP, Potter KD. Exploring the pseudo-ductility of aligned hybrid discontinuous composites using controlled fibre-type arrangements. Compos Part A Appl Sci Manuf 2018;107:592–606. https://doi.org/10.1016/j.compositesa.2017.11.028.

[10] Fuller JDD, Wisnom MRR. Ductility and pseudo-ductility of thin ply angle-ply CFRP laminates under quasi-static cyclic loading. Compos Part A Appl Sci Manuf 2018;107:31–8. https://doi.org/10.1016/j.compositesa.2017.12.020.

[11] Yuan Y, Wang S, Yang H, Yao X, Liu B. Analysis of pseudo-ductility in thin-ply carbon fiber angle-ply laminates. Compos Struct 2017;180:876–82. https://doi.org/10.1016/j.compstruct.2017.08.070.

[12] Fuller JDD, Wisnom MRR. Pseudo-ductility and damage suppression in thin ply CFRP angle-ply laminates. Compos Part A Appl Sci Manuf 2015;69:64–71. https://doi.org/10.1016/j.compositesa.2014.11.004.

[13] Yu H, Potter KDD, Wisnom MRR. A novel manufacturing method for aligned discontinuous fibre composites (High Performance-Discontinuous Fibre method). Compos Part A Appl Sci Manuf 2014;65:175–85. https://doi.org/10.1016/j.compositesa.2014.06.005.

[14] Longana ML, Yu HN, Jalavand M, Wisnom MR, Potter KD. Aligned discontinuous intermingled reclaimed/virgin carbon fibre composites for high performance and pseudo-ductile behaviour in interlaminated carbon-glass hybrids. Compos Sci Technol 2017;143:13–21. https://doi.org/10.1016/j.compscitech.2017.02.028.

[15] Yu H, Longana ML, Jalalvand M, Wisnom MR, Potter KD. Pseudo-ductility in intermingled carbon/glass hybrid composites with highly aligned discontinuous fibres. Compos Part A Appl Sci Manuf 2015;73:35–44. https://doi.org/10.1016/j.compositesa.2015.02.014.

[16] Zucchelli A, Focarete ML, Gualandi C, Ramakrishna S. Electrospun nanofibers for enhancing structural performance of composite materials. Polym Adv Technol 2011;22:339–49. https://doi.org/10.1002/pat.1837.

[17] Molnár K, Košťáková E, Mészáros L. The effect of needleless electrospun nanofibrous interleaves on mechanical properties of carbon fabrics/epoxy laminates. Express Polym Lett 2014;8:62–72. https://doi.org/10.3144/expresspolymlett.2014.8.

[18] Palazzetti R, Zucchelli A. Electrospun nanofibers as reinforcement for composite laminates materials – a review. Compos Struct 2017;182:711–27. https://doi.org/10.1016/j.compstruct.2017.09.021.

[19] Koprivova B, Lisnenko M, Solarska-Sciuk K, Prochazkova R, Novotny V, Mullerova J, et al. Large-scale electrospinning of poly (Vinylalcohol) nanofibers incorporated with platelet-derived growth factors. Express Polym Lett 2020;14:987–1000. https://doi.org/10.3144/expresspolymlett.2020.80.

[20] Salehi MM, Hakkak F, Sadati Tilebon SM, Ataeefard M, Rafizadeh M. Intelligently optimized electrospun polyacrylonitrile/poly(vinylidene fluoride) nanofiber: using artificial neural networks. Express Polym Lett 2020;14:1003–17. https://doi.org/10.3144/expresspolymlett.2020.82.

[21] Lomov SV, Molnár K. Compressibility of carbon fabrics with needleless electrospun PAN nanofibrous interleaves. Express Polym Lett 2016;10:25–35. https://doi.org/10.3144/expresspolymlett.2016.4.

[22] Ou Y, González C, Vilatela JJ. Interlaminar toughening in structural carbon fiber/epoxy composites interleaved with carbon nanotube veils. Compos Part A Appl Sci Manuf 2019;124:105477. https://doi.org/10.1016/j.compositesa.2019.105477.

[23] Kostagiannakopoulou C, Tsilimigkra X, Sotiriadis G, Kostopoulos V. Synergy effect of carbon nano-fillers on the fracture toughness of structural composites. Compos Part B Eng 2017;129:18–25. https://doi.org/10.1016/j.compositesb.2017.07.012.

[24] Romhány G, Szebényi G. Interlaminar crack propagation in MWCNT/fiber reinforced hybrid composites. Express Polym Lett 2009;3:145–51. https://doi.org/10.3144/expresspolymlett.2009.19.

[25] Romhány G, Szebényi G. Interlaminar fatigue crack growth behavior of MWCNT/carbon fiber reinforced hybrid composites monitored via newly developed acoustic emission method. Express Polym Lett 2012;6:572–80. https://doi.org/10.3144/expresspolymlett.2012.60.

[26] Yun NG, Won YG, Kim SC. Toughening of carbon fiber/epoxy composite by inserting polysulfone film to form morphology spectrum. Polymer (Guildf) 2004;45:6953–8. https://doi.org/10.1016/J.POLYMER.2004.08.020.

[27] Naffakh M, Dumon M, Gérard JF. Study of a reactive epoxy–amine resin enabling in situ dissolution of thermoplastic films during resin transfer moulding for toughening composites. Compos Sci Technol 2006;66:1376–84. https://doi.org/10.1016/J.COMPSCITECH.2005.09.007.

[28] Shivakumar K, Panduranga R. Interleaved polymer matrix composites - a review. In: 54th AIAA/ASME/ASCE/AHS/ASC Struct. Struct. Dyn. Mater. Conf., Boston, Massachusetts: American Institute of Aeronautics and Astronautics; 2013. https://doi.org/10.2514/6.2013-1903.

[29] Qian X, Kravchenko OG, Pedrazzoli D, Manas-Zloczower I. Effect of polycarbonate film surface morphology and oxygen plasma treatment on mode I and II fracture toughness of interleaved composite laminates. Compos Part A Appl Sci Manuf 2018;105:138–49. https://doi.org/10.1016/j.compositesa.2017.11.016.

[30] Grail G, Pimenta S, Pinho ST, Robinson P. Exploring the potential of interleaving to delay catastrophic failure in unidirectional composites under tensile loading. Compos Sci Technol 2015;106:100–9. https://doi.org/10.1016/j.compscitech.2014.11.006.

[31] Evans R, Masters J, RE Evans JEM. A new generation of epoxy composites for primary structural applications: materials and mechanics. In: Johnston NJ, editor. Toughened Compos., West Conshohocken, PA: ASTM International; 1987. p. 413-413–24. https://doi.org/10.1520/STP24391S.

[32] Anthony DB, Bacarreza Nogales OR, Shaffer MSP, Bismarck A, Robinson P, Pimenta S. Pseudo-ductile failure mechanism introduced into finger jointed thermoplastic PES interleaved CFRC. In: ECCM 2018 - 18th Eur. Conf. Compos. Mater., Athens, Greece; 2020.

[33] Hodgkin JH, Simon GP, Varley RJ. Thermoplastic toughening of epoxy resins: a critical review. Polym Adv Technol 1998;9:3–10. https://doi.org/10.1002/(SICI)1099-1581(199801)9:1<3::AID-PAT727>3.0.CO;2-I.

[34] Nash NH, Young TM, McGrail PT, Stanley WF. Inclusion of a thermoplastic phase to improve impact and post-impact performances of carbon fibre reinforced thermosetting composites - a review. Mater Des 2015;85:582–97. https://doi.org/10.1016/j.matdes.2015.07.001.

[35] Li L, Lee-Sullivan P, Liew KM. The influence of thermoplastic film interleaving on the interlaminar shear strength and mode i fracture of laminated composites. J Eng Mater Technol Trans ASME 1996. https://doi.org/10.1115/1.2806810.

[36] Kim JW, Lee JS. Influence of interleaved films on the mechanical properties of carbon fiber fabric/polypropylene thermoplastic composites. Materials (Basel) 2016;9. https://doi.org/10.3390/ma9050344.

[37] Singh S, Partridge IK. Mixed-mode fracture in an interleaved carbon-fibre/epoxy composite. Compos Sci Technol 1995;55:319–27. https://doi.org/10.1016/0266-3538(95)00062-3.

[38] Hojo M, Ando T, Tanaka M, Adachi T, Ochiai S, Endo Y. Modes I and II interlaminar fracture toughness and fatigue delamination of CF/epoxy laminates with self-same epoxy interleaf. Int J Fatigue 2006;28:1154–65. https://doi.org/10.1016/J.IJFATIGUE.2006.02.004.

[39] Wang CH, Sidhu K, Yang T, Zhang J, Shanks R. Interlayer self-healing and toughening of carbon fibre/epoxy composites using copolymer films. Compos Part A Appl Sci Manuf 2012;43:512–8. https://doi.org/10.1016/j.compositesa.2011.11.020.

[40] Varley RJ, Craze DA, Mouritz AP, Wang CH. Thermoplastic healing in epoxy networks: Exploring performance and mechanism of alternative healing agents. Macromol Mater Eng 2013;298:1232–42. https://doi.org/10.1002/mame.201200394.

[41] Cano J, Torres A, Abad MJ, Barral L, Díez FJ, López J, et al. Characterization of an ABS-modified epoxy system. Polym Int 2002;51:1268–76. https://doi.org/10.1002/pi.940.

[42] López J, Ramírez C, Abad MJ, Barral L, Cano J, Díez FJ. Blends of acrylonitrile-butadiene-styrene with an epoxy/cycloaliphatic amine resin: phase-separation behavior and morphologies. J Appl Polym Sci 2002;85:1277–86. https://doi.org/10.1002/app.10715.

[43] Abad MJ, Barral L, Cano J, López J, Nogueira P, Ramírez C, et al. Thermal decomposition behavior and the mechanical properties of an epoxy/cycloaliphatic amine resin with ABS. Eur Polym J 2001;37:1613–23. https://doi.org/10.1016/S0014-3057(01)00036-2.

[44] Natarajan K, Rao RMVGK. Toughening studies on an ABS/PC blend-modified epoxy resin system. High Perform Polym 1994;6:241–8. https://doi.org/10.1088/0954-0083/6/3/007.

[45] Tsuchikura N, Faudree MC, Nishi Y. Charpy Impact Value of Sandwich Structural (CFRP/ABS/CFRP) Composites Constructed with Carbon Fiber Reinforced Epoxy Polymer (CFRP) and Acrylonitrile Butadiene Styrene (ABS) Sheets Separately Irradiated by Electron Beam Prior to Lamination. Mater Trans 2013;54:371–9. https://doi.org/10.2320/matertrans.MBW201209.

[46] Tridech C, Maples HA, Robinson P, Bismarck A. High performance composites with active stiffness control. ACS Appl Mater Interfaces 2013;5:9111–9. https://doi.org/10.1021/am402495n.

[47] Maples HA, Wakefield S, Robinson P, Bismarck A. High performance carbon fibre reinforced epoxy composites with controllable stiffness. Compos Sci Technol 2014;105:134–43. https://doi.org/10.1016/j.compscitech.2014.09.008.

[48] Swolfs Y, Gorbatikh L, Verpoest I. Fibre hybridisation in polymer composites: a review. Compos Part A Appl Sci Manuf 2014;67:181–200. https://doi.org/10.1016/j.compositesa.2014.08.027.

[49] Jalalvand M, Czél G, Wisnom MR. Numerical modelling of the damage modes in UD thin carbon/glass hybrid laminates. Compos Sci Technol 2014;94:39–47. https://doi.org/10.1016/j.compscitech.2014.01.013.

[50] Jalalvand M, Czél G, Wisnom MR. Damage mode maps and parametric study of thin UD hybrid composites. In: 16th Eur. Conf. Compos. Mater. ECCM 2014, Seville, Spain; 2014. p. 22–6.

[51] Jalalvand M, Czél G, Wisnom MR. Damage analysis of pseudo-ductile thin-ply UD hybrid composites - a new analytical method. Compos Part A Appl Sci Manuf 2015;69:83–93. https://doi.org/10.1016/j.compositesa.2014.11.006.

[52] Wisnom MR. On the increase in fracture energy with thickness in delamination of unidirectional glass fibre-epoxy with cut central plies. J Reinf Plast Compos 1992;11:897–909. https://doi.org/10.1177/073168449201100802.

[53] Cui W, Wisnom MR, Jones M. An experimental and analytical study of delamination of unidirectional specimens with cut central plies. J Reinf Plast Compos 1994;13:722–39. https://doi.org/10.1177/073168449401300804.

[54] Rev T, Jalalvand M, Fuller J, Wisnom MR, Czél G. A simple and robust approach for visual overload indication - UD thin-ply hybrid composite sensors. Compos Part A Appl Sci Manuf 2019;121:376–85. https://doi.org/10.1016/J.COMPOSITESA.2019.03.005.

[55] Wisnom MR, Czél G, Swolfs Y, Jalalvand M, Gorbatikh L, Verpoest I. Hybrid effects in thin ply carbon/glass unidirectional laminates: Accurate experimental determination and prediction. Compos Part A Appl Sci Manuf 2016;88:131–9. https://doi.org/10.1016/j.compositesa.2016.04.014.

[56] Swolfs Y, Verpoest I, Gorbatikh L. Recent advances in fibre-hybrid composites: materials selection, opportunities and applications. Int Mater Rev 2019;64:181–215. https://doi.org/10.1080/09506608.2018.1467365.

[57] Czél G, Jalalvand M, Wisnom MR. Hybrid specimens eliminating stress concentrations in tensile and compressive testing of unidirectional composites. Compos Part A Appl Sci Manuf 2016;91:436–47. https://doi.org/10.1016/j.compositesa.2016.07.021.

[58] Laws N, Dvorak GJ. The effect of fiber breaks and aligned penny-shaped cracks on the stiffness and energy release rates in unidirectional composites. Int J Solids Struct 1987;23:1269–83. https://doi.org/10.1016/0020-7683(87)90105-3.

[59] Beyerlein IJ, Phoenix SL. Stress profiles and energy release rates around fiber breaks in a lamina with propagating zones of matrix yielding and debonding. Compos Sci Technol 1997;57:869–85. https://doi.org/10.1016/S0266-3538(96)00178-9.

[60] Behzadi S, Curtis PT, Jones FR. Improving the prediction of tensile failure in unidirectional fibre composites by introducing matrix shear yielding. Compos Sci Technol 2009;69:2421–7. https://doi.org/10.1016/j.compscitech.2009.06.010.

[61] Davies P, Casari P, Carlsson LA. Influence of fibre volume fraction on mode II interlaminar fracture toughness of glass/epoxy using the 4ENF specimen. Compos Sci Technol 2005;65:295–300. https://doi.org/10.1016/j.compscitech.2004.07.014.